Journal of Applied Electrochemistry **32**: 1347–1353, 2002.

A zinc–air cell employing a porous zinc electrode fabricated from zinc–graphite-natural biodegradable polymer paste

R. OTHMAN[1], A.H. YAHAYA[2] and A.K. AROF[3,*]
[1]*Department of Science in Engineering, International Islamic University Malaysia, 53100 Kuala Lumpur, Malaysia;*
[2]*Department of Chemistry, University of Malaya, 50603 Kuala Lumpur, Malaysia;*
[3]*Department of Physics, University of Malaya, 50603 Kuala Lumpur, Malaysia;*
*(*author for correspondence, e-mail: akarof@um.edu.my)*

Received 14 February 2002; accepted in revised form 20 August 2002

Key words: agar solution, hydroponics gel, KOH electrolyte, natural polymer binder, porous zinc anode, zinc–air cell

Abstract

Porous zinc anodes have been fabricated from a mixture of zinc and graphite powder using gelatinized agar solution as the binding agent. Agar is a biodegradable polysaccharide polymer extracted from marine algae. The graphite content and the agar solution concentration were varied to find the best electrode composition. Zinc–air cells were fabricated using the porous zinc anode, a commercially available air cathode sheet and KOH electrolyte in the form of elastic jelly granules. The electrode performance was evaluated from the zinc–air cell galvanostatic discharge capability. In the cell design, a thin agar layer was introduced between the electrode-gelled electrolyte interfaces, resulting in substantially improved cell discharge performance. The inclusion of particulate graphite into the electrode did not enhance the electrode performance due to the formation of a graphite-rich layer, which obscured the electrode porosity. A zinc–air cell employing the optimized porous zinc electrode demonstrated a capacity of 2066 mA h and specific energy density of 443 Wh kg^{-1}.

1. Introduction

One of the major factors that governs anode mass utilization, and thus the specific energy density of an electrochemical power source, is its surface area. A higher surface area per unit volume for a given amount of active material decreases the current density and leads to an increase in the electrode rate capability and active material utilization [1]. Porous electrodes remain the centre of interest in the development of batteries and fuel cells due to the efficient and high surface area obtained [2–9]. By providing an enhanced and intimate interfacial area per unit volume, the porous electrode increases the kinetics and mass transfer of the electrochemical reaction thus minimizing the energy loss [10].

Porous zinc anodes are prepared in various ways such as; electrodeposited from an aqueous electrolytic bath [11, 12]; roll-bonded process where a mixture of zinc, graphite, binder and solvent is extruded into a thin sheet [13]; compressed dry powder process where a powder mixture of zinc and binder is placed in a mold and compressed around a current collector [12, 14]; and paste or slurry preparation technique where powdered zinc oxide with gelling agent is mixed with KOH solution to form a paste and later applied onto a metal grid, dried and formed against a positive electrode in KOH solution [15–17].

We have reported a preliminary study on a porous zinc electrode fabricated from a zinc and graphite powder mixture utilizing a thick gelatinous agar solution as binder, and applying it in the zinc–air cell. A 1470 mA h zinc–air cell of monopolar design has been demonstrated [18]. In that work, however, we did not optimize the electrode composition, namely the graphite content and agar solution concentration. Following the promising results obtained [18], we have, in the present work, optimized the electrode composition by varying its graphite content and the concentration of the agar solution. Graphite was included in the electrode composition in view of its favourable effects on the zinc electrode reported by several workers [19–21]. The inclusion of conductive particulate graphite was reported to improve the zinc anode discharge capability, considerably inhibit active zinc dissolution and promote reprecipitation of oxidized zinc species [19–21]. The fabricated zinc electrodes were assembled into zinc–air cells and their performance was evaluated from the galvanostatic discharge curve. The porous zinc electrode preparation technique adapted in this work is simple and fast, uses environmentally benign and biodegradable binding material, does not require either elevated

heat treatment or a mould and hydraulic press. In the zinc–air cell design, a thin KOH-treated agar layer was applied between the electrode and gelled electrolyte to improve the interfacial contact. In the previous study on the zinc–air cell employing planar zinc foil as the anode, the application of a thin agar layer between the electrode-gelled electrolyte interfaces enhanced the cell discharge capabilities considerably [18, 22]. We demonstrate here that though the porous anode possesses a high surface area and sufficient amounts of KOH electrolyte normally entrapped within the electrode pores, the application of the thin agar layer between the electrode-gelled electrolyte interfaces is still beneficial to the cell discharge performance.

1.1. *Some properties of agar*

Agar is a biodegradable polysaccharide polymer extracted from marine algae and is hydrophilic in nature. It comprises mainly neutral polymer agarose, pyruvated agarose and sulphated galactans. The structure of agar is based on a disaccharide alternating repeat structure of 3-linked β-D-galactopyranosyl and 4-linked 3,6-anhydro-α-L-galactopyranosyl units [23–27]. The gel forming properties of agar have found useful applications in the medical, agricultural, drug packaging and release, cosmetics and food industries [28]. Other types of polysaccharides, namely cellulose and its derivatives, and starch, have been widely used in materials applications [29–32].

1.2. *Reaction mechanisms of the zinc–air cell*

The overall zinc–air cell reactions can be summarized as follows [33, 34]:
Cathodic reaction

$$O_2 + 2\ H_2O + 4\ e^- \rightarrow 4OH^- \quad E^\circ = 0.40\,V$$

Anodic reaction

$$2\ Zn \rightarrow 2\ Zn^{2+} + 4e^-$$

$$2\ Zn^{2+} + 4\ OH^- \rightarrow 2\ Zn(OH)_2 \quad E^\circ = 1.25\,V$$

$$2\ Zn(OH)_2 \rightarrow 2\ ZnO + 2\ H_2O$$

Overall Reaction

$$2\ Zn + O_2 \rightarrow 2\ ZnO \quad E^\circ = 1.65\,V$$

Based on the theoretical cell voltage of 1.65 V and assuming the final reaction product is ZnO, the theoretical specific energy density of the zinc–air cell is 1085 Wh kg^{-1} [35–37].

2. Experimental details

2.1. *Fabrication of the porous zinc electrode*

A mixture of zinc and graphite powder was employed. The amount of graphite included was varied from initially 20 wt % and finally reduced to 0 wt %, whereas the amount of zinc powder used was fixed at 4.5 g. The zinc–graphite powder mixture was blended with 4 ml of gelatinized agar solution to form a paste. The preparation of the gelatinized agar solution is described below. We employed a 5 mg cm^{-3} agar solution concentration. The anode paste was then cast onto a nickel-plated mesh that had been snugly fitted to a plastic holder and finally dried at a temperature of 50 °C. The dried gelatinized agar solution acts as binder to the zinc–graphite powder mixture. We also used an agar concentration of 15 mg cm^{-3} and 25 mg cm^{-3} on the optimized zinc–carbon electrode composition.

2.2. *Preparation of the gelatinized agar solution*

Purified agar (Bacto-Agar) in fine granular form was mixed with deionized water, stirred and dissolved at 90 °C to give a clear solution. The agar solution was left to cool and gelatinize at room temperature.

2.3. *Zinc–air cell assembly and design*

The primary zinc–air cell was assembled in the monopolar arrangement. It comprised the fabricated porous zinc anode, a commercially available carbon-based air cathode sheet that consisted of laminated structures of fibrous carbon supported by a nickel-plated mesh and a 2.8 M aqueous potassium hydroxide electrolyte immobilized with hydroponics gel. We introduced hydroponics gel as a new alkaline electrolyte-immobilizing agent [38]. The cell components were enclosed in a cylindrical plastic casing 28 mm in height and 45 mm in diameter. Figure 1 depicts the construction of the components into a complete cell. Details of cell fabrication and components are given elsewhere [18, 22, 38]. Normally zinc anode batteries comprise an aqueous KOH concentration in the range 6–10 M (27 to 40 wt %) [39]. As the 2.8 M KOH concentration employed in this work was comparatively low, we also employed a KOH concentration of 6.0 M.

In the cell, a thin KOH-treated agar layer was applied between the electrode–electrolyte interfaces to improve the electrode–electrolyte interfaces and simultaneously to serve as the electrolyte reservoir to both electrodes. We have reported a marked zinc–air cell capacity enhancement when a thin KOH-treated agar layer was applied to the electrodes [18, 22]. However, in the previous work a simple classical cell design was adopted, whereby a compact planar zinc foil was used as anode. In the present work, a zinc–air cell was prepared in which (a) both the porous zinc anode and the air cathode were coated with a thin agar layer, (b) only the porous zinc anode was coated and finally (c) no agar layer was applied to either electrode.

2.4. *Characterization of the zinc–air cell*

The zinc–air cell operating voltage was measured as a function of galvanostatic current drains from 10 μA to

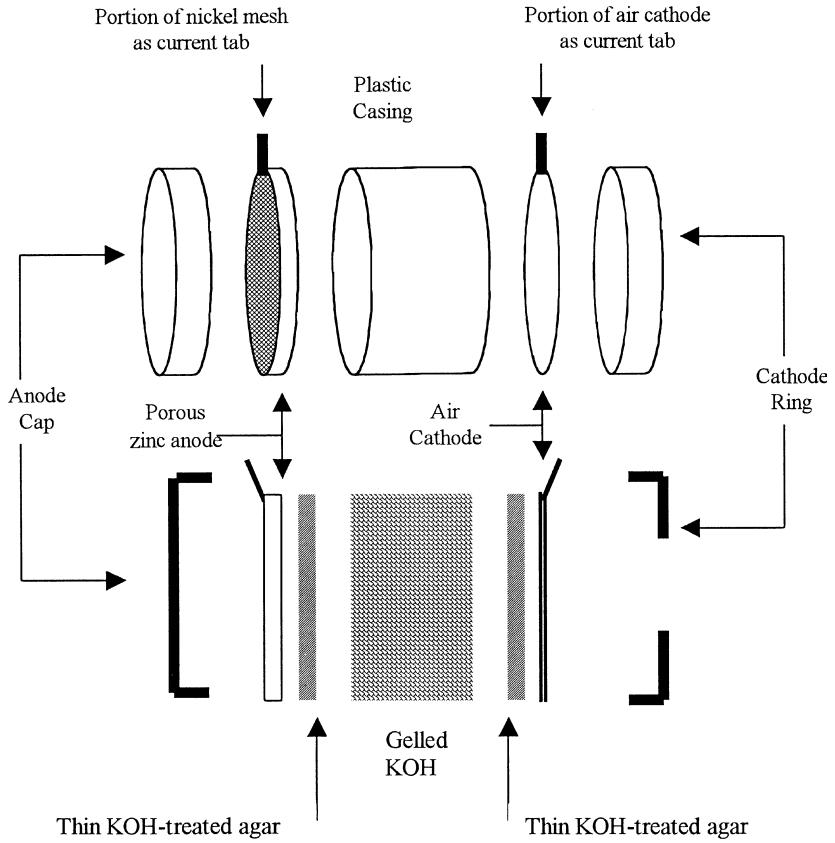

Fig. 1. Layout of the zinc–air cell assembly and its components.

100 mA. Values of cell voltage for each particular current drain were monitored for 10 s and the average value was recorded. The respective power density profile of the cell was calculated from the measured voltage–current curve. The zinc–air cell was discharged to 100% DOD at constant currents of 50 and 100 mA. A LG-50 galvanostat electroanalytical system was used to control the experiments.

2.5. *Characterization of the porous zinc anode*

SEM micrographs, X-ray diffraction measurement and particle size analysis were also performed on the porous zinc anode. The SEM micrographs were recorded using an Oxford 5431 SEM instrument. XRD measurements were taken using a Philips X-ray diffractometer XD-5 with CuK_α radiation (154.05 pm). The particle size distribution of the zinc and graphite powders was analyzed using a Coulter LS 230 particle size analyser.

3. Results and discussion

The mean particle sizes of the zinc and graphite powders used in the fabrication of the porous electrode were 12 and 18 μm, respectively. Figure 2a displays a cross sectional view of the porous electrode consisting of a mixture of zinc and graphite powder. Two distinct layers are apparent. Closer observation of the darker region

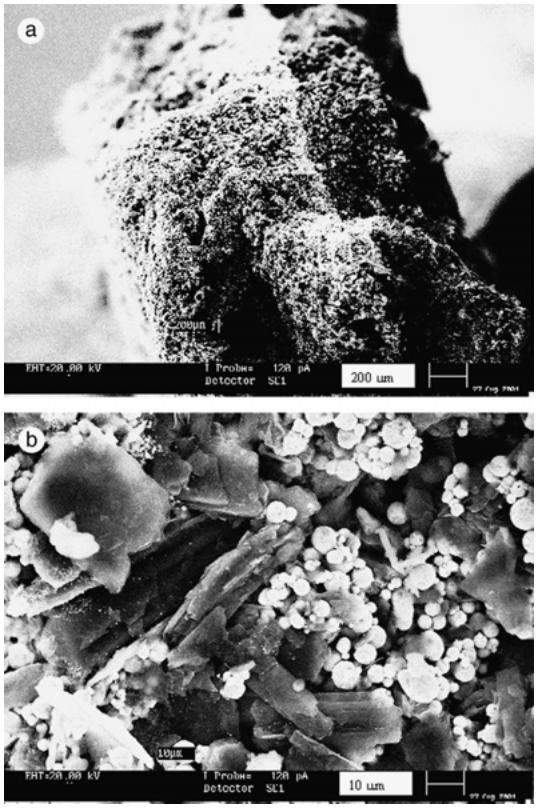

Fig. 2. SEM cross-sectional micrographs of the porous zinc anode fabricated from a mixture of zinc and graphite powder.

reveals that it is a graphite-rich matrix (Figure 2(b)). Figures 3(a) and (b) show a cross-sectional view of the porous zinc electrode consisting of zinc powder only at different magnifications. Note the whitish trace of the dried agar that acts as a binder to the zinc powder.

The fabricated porous zinc electrode was assembled into the zinc–air cell and its performance was evaluated from the cell discharge capability. The average open circuit potential was 1.42 V. The discharge performance, as the graphite content of zinc electrode was varied, is shown in Figure 4. The cell capacity has a maximum of 1349 mA h when the graphite content in the zinc electrode is zero. The cell capacity decreases as the graphite content increases up to 10 wt %, after which it is constant.

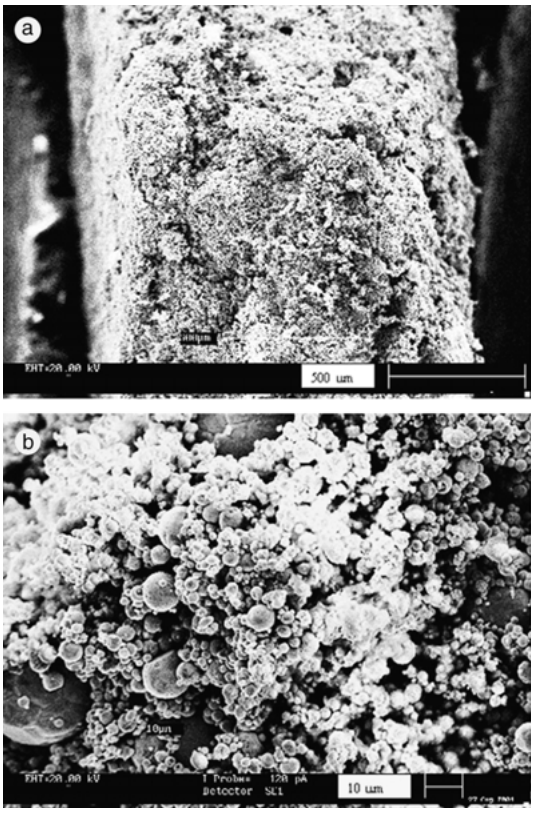

Fig. 3. SEM cross-sectional view of the optimized porous zinc anode that consists of zinc powder only.

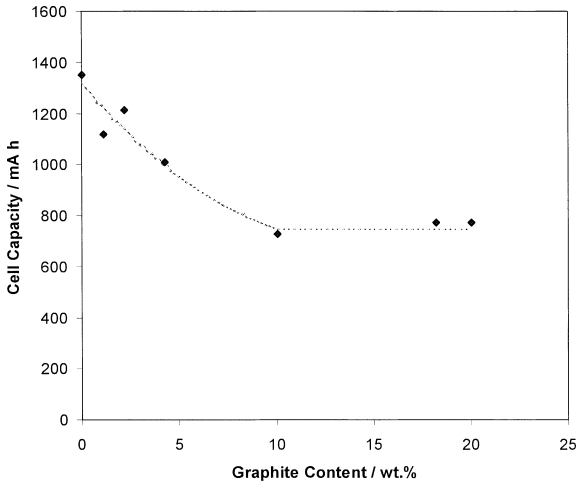

Fig. 4. Effect of graphite content in porous zinc anode on zinc–air cell capacity.

Duffield et al. [19] and Lucas Industries [20] have reported favourable results on the inclusion of particulate graphite into the zinc electrode. The conductive particulate graphite was reported to improve zinc anode discharge capability, considerably inhibit active zinc dissolution and promote reprecipitation of oxidized zinc species [19–21]. However, in the present work, an optimum cell capacity of 1349 mA h was obtained for the electrode without graphite content and the cell capacity decreased with increasing graphite content. We attribute these results to the existence of two distinct layers in the electrode structure and the gelled type electrolyte. Graphite, with its density significantly lower than zinc, surfaces and forms a graphite-rich matrix in the electrode structure. As a result, the formation of the graphite-rich layer obscures the electrode wettability and porosity, and reduces the cell capacity. The use of gelled KOH in the form of semisolid jelly granules further exacerbates this phenomenon due to the limited free electrolyte of the gelled electrolyte. The use of a flooded type cell [19–21] would probably produce a contrasting result.

Another factor that might contribute to the formation of the graphite-rich layer is the agar solution concentration. A more viscous gelatinized agar solution most probably blends the zinc and graphite mixture homogeneously. Nevertheless, the electrode fabricated from zinc powder using higher agar solution concentrations of 15 mg cm^{-3} and 25 mg cm^{-3} resulted in reduced cell capacity, though it improved the electrode mechanical stability and strength. Figure 5 displays the galvanostatic discharge curves of a cell employing a porous zinc anode fabricated from agar solutions of concentrations 5, 15 and 25 mg cm^{-3}, in which no graphite was incorporated into the electrode. It clearly shows that

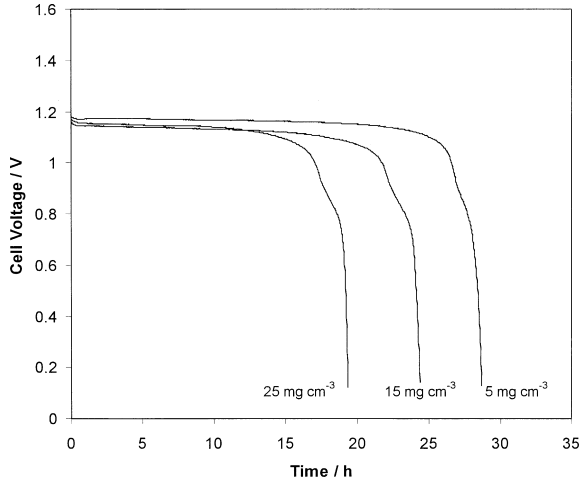

Fig. 5. Zinc–air cell discharge performance as a function of agar solution concentration used in the preparation of the porous zinc anode.

the best discharge performance is obtained from the zinc anode with 5 mg cm^{-3} agar. Below 5 mg cm^{-3}, the resulting solution was too dilute and watery and was not applied in electrode fabrication. At these solution concentrations, the dried agar forms a film that is thick enough to shield the zinc active material and thus reduce the cell capacity. Figure 6(a) depicts the SEM cross-sectional micrograph of the porous zinc electrode employing a higher agar solution concentration of 15 mg cm^{-3} concentration of 15 mg cm^{-3}, which clearly showed this. Note the film formed from the dried agar solution on the upper right-hand corner of the micrograph, which encapsulated some portion of the electrode active material. Figure 6(b) gives a clearer view at higher magnification taken from other spots.

For comparison, the cell was also fabricated using a 0.4 mm thick zinc foil as anode with an equivalent weight and cell design. Figure 7 shows the outstanding discharge performance of the cell employing a porous zinc anode compared to that utilizing compact planar zinc foil at 50 mA constant current drain. These results were obtained with an aqueous KOH concentration of 2.8 M, which was lower than that normally employed in alkaline zinc anode batteries [39]. Therefore, zinc–air cells were fabricated utilizing the optimized porous zinc electrode composition and employing a higher KOH concentration of 6 M. Figure 8 depicts the discharge performances at 50 and 100 mA, respectively, employing 2.8 and 6 M KOH. As anticipated, an enhanced discharge capability was obtained at higher concentration. With 6 M KOH, the cell capacity was 2066 and 1910 mA h, for 50 and 100 mA, respectively. Figure 9 shows the profile of operating voltage as a function of current drain of a cell employing the optimized porous zinc anode at different KOH concentrations, and also shows the corresponding power density gain against current drain curve.

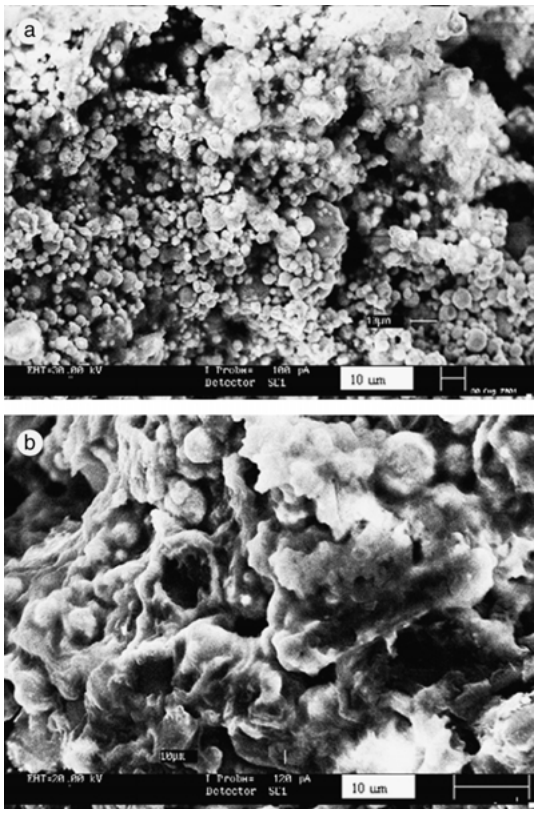

Fig. 6. SEM micrographs showing the formation of agar film that shields some portion of the zinc active material.

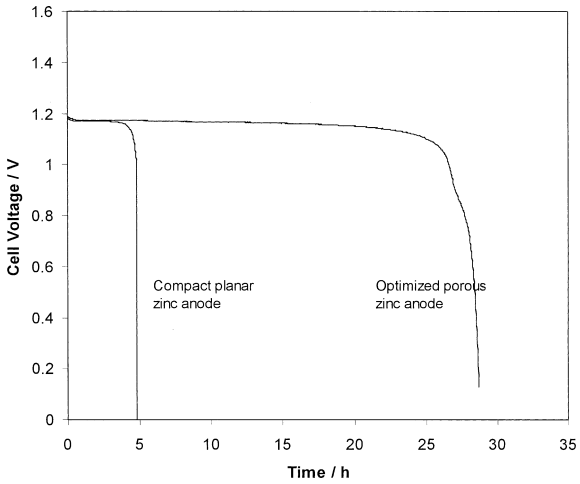

Fig. 7. Discharge performance of the zinc–air cell employing the optimized porous zinc anode as compared to that using a compact planar zinc foil.

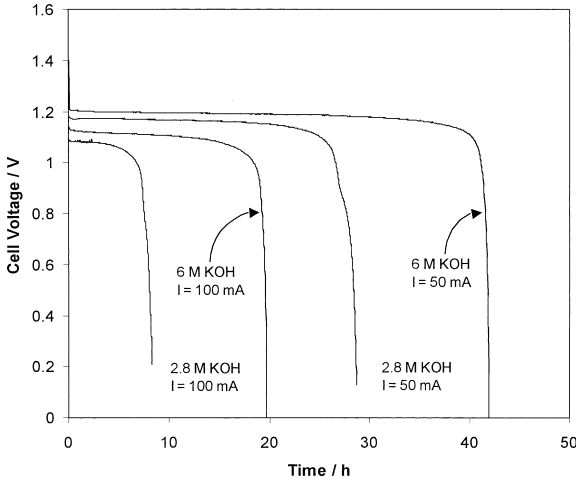

Fig. 8. Zinc–air cell discharge profiles at 50 and 100 mA employing 2.8 and 6 M KOH concentrations, respectively.

The porosity of the optimized zinc electrode was found to be approximately around 60%. The thickness of the optimized porous zinc electrode was about 1.0 mm as estimated from the SEM micrograph. Thus, the calculation is as follows:

$$\text{Porosity} = \frac{V_{\text{Pore}}}{V_{\text{Total}}} \times 100\% = \left(\frac{V_{\text{Total}} - V_{\text{Zn}}}{V_{\text{Total}}}\right) \times 100\% = \left(1 - \frac{m_{\text{Zn}}/\rho_{\text{Zn}}}{\pi r^2 h}\right) \times 100\%$$

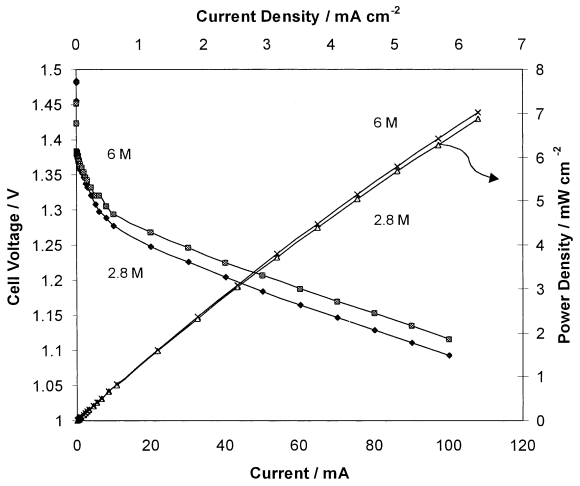

Fig. 9. Zinc–air cell operating voltage as a function of constant current drain profiles at 2.8 and 6 M electrolyte concentrations and the corresponding power density profiles.

where V_{pore} is the total pore volume within the electrode, V_{Total} the total electrode volume, V_{Zn} the total volume occupied by the zinc active material, m_{Zn} the zinc active material total mass, ρ_{Zn} the zinc density (7.13 g cm^{-3}); r and h are the electrode radius and thickness, respectively.

The application of a thin agar layer between the electrode-gelled electrolyte interfaces essentially improves the cell discharge performance. As shown in Figure 10, the cell capacity improved by 28% when an agar layer was introduced between the zinc anode-gelled electrolyte interface, and was further enhanced by 52% when the agar layer was applied to both electrode-gelled electrolyte interfaces. These profiles were obtained at 100 mA discharge current employing a 6 M KOH electrolyte. The agar layer promotes a better interfacial contact between the electrode and the gelled electrolyte. Although the fabricated zinc electrode was highly porous – thus contributing to a high specific surface area as the KOH electrolyte was in the form of loosely bound elastic jelly granules – it may possibly contribute to higher cell impedance. Vinod and Vijayamohanan [40], applying impedance spectroscopy, verified that the gelling of the electrolyte in the maintenance-free lead acid battery causes a considerable increase in the interfacial ohmic resistance and the electrolyte diffusion transport impedance. Another notable feature of diffusion transport in gels is the existence of simultaneously competitive diffusion and retention processes [41]. Algal polysaccharides are fibrous materials with gel forming properties. Agar is also known in its natural form as serving as a water reservoir in algal cell walls [42, 43]. Thus we anticipate that although agar layer improves the electrode-gelled electrolyte interfacial contact, it also serves as an electrolyte reservoir and maintains the wettability of the electrodes. Nevertheless, more elaborate studies are needed to support these observations.

SEM micrographs of the post-discharge electrode show that the zinc particles are covered with crystals, possibly of zinc oxide (Figure 11). The XRD diffractogram of the post-discharge electrode as depicted in Figure 12, matches that of zinc oxide [44, 45], which confirms the SEM observations. Zinc oxide is the end product of the zinc–air cell electrochemical reaction.

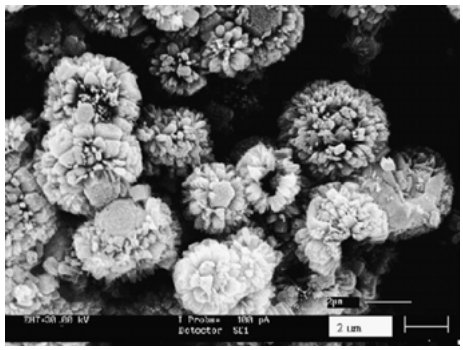

Fig. 11. Post-discharge SEM micrographs of the porous zinc electrode exhibit the zinc particles are covered with zinc oxide crystals.

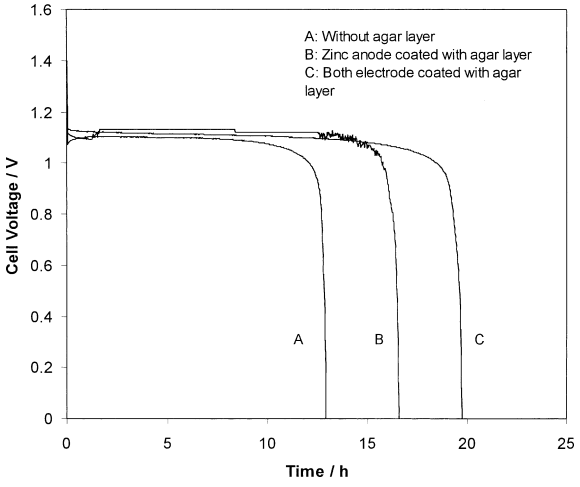

Fig. 10. Discharge profiles demonstrating the beneficial effects of applying a thin agar layer between the electrode-gelled electrolyte interfaces.

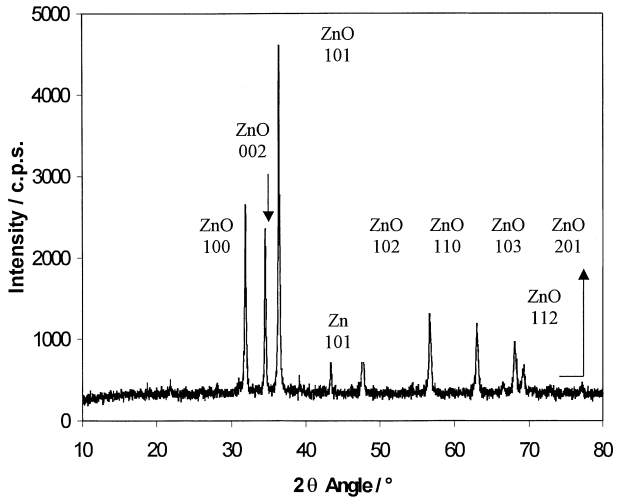

Fig. 12. XRD diffractogram of the post-discharge porous zinc anode that matches to that of zinc oxide.

We have demonstrated 1910 mA h (420 Wh kg^{-1}) and 2066 mA h (443 Wh kg^{-1}) capacities for a single 1.4 V zinc–air cell rated at continuous current drains of 0.1 A and 50 mA, respectively, which is comparable to present zinc–air batteries. For example, Electric Fuel Ltd recently introduced a 3.6 V primary zinc–air battery for cellular phones rated at 3300 mA h [46]. Based on the 4.5 g (4.5/65.37 mol) zinc active material and considering zinc oxide (81.37×10^{-3} kg mol^{-1}) as the end product of the electrochemical reaction, the cell specific energy density ($E_{specific}$) is calculated as follows:

$$E_{specific} = \frac{[practical\ cell\ capacity(Ah)] \times [average\ operating\ voltage\ (V)]}{[amount\ of\ discharge\ product\ (kg)]}$$

4. Conclusions

A porous zinc anode of 60% porosity has been fabricated from zinc powder using gelatinized algal polysaccharide solution as a binder. The technique employed is simple, fast and requires neither elevated heat treatment nor a mould and hydraulic press. At 5 mg cm^{-3} agar solution concentration, the inclusion of particulate graphite into the electrode does not improve its performance. The particulate graphite surfaces and forms a graphite-rich layer that diminishes electrode porosity. The application of a thin agar layer between the electrode-gelled electrolyte interfaces improves the cell discharge performance significantly. A zinc–air cell employing the optimized porous electrode has demonstrated a practical capacity of 2066 mA h and specific energy density of 443 Wh kg^{-1}.

References

1. N.E. Bagshaw, *J. Power Sources* **67** (1997) 105.
2. J.J. Kriegsmann and H.Y. Cheh, *J. Power Sources* **77** (1999) 127.
3. X. Jin and J. Lu, *J. Power Sources* **93** (2001) 8.
4. C.A. Marozzi and A.C. Chialvo, *Electrochim. Acta* **45** (2000) 2111.
5. P. Novak, W. Scheifele, M. Winter and O. Haas, *J. Power Sources* **68** (1997) 267.
6. P. Periasamy, B.R. Babu and S.V. Iyer, *J. Power Sources* **58** (1996) 35.
7. G. Lindbergh, *Electrochim. Acta* **42** (1997) 1239.
8. A. Lasia, *J. Electroanal. Chem.* **428** (1997) 155.
9. A. Lasia, *J. Electroanal. Chem.* **397** (1995) 27.
10. J. Newman and W. Tiedemann, *AIChE J.* **21** (1975) 25.
11. P.A. Barbic, L. Binder, S. Voss, F. Hofer and W. Grogger, *J. Power Sources* **79** (1999) 271.
12. A. Himy, Silver-Zinc Battery: Phenomena and Design Principles, 1st edn (Vantage Press, 1986), p. 28.
13. D. Coates, E. Ferreira and A. Charkey, *J. Power Sources* **65** (1997) 109.
14. J.L. Zhu and Y.H. Zhou, *J. Power Sources* **73** (1998) 266.
15. R. Shivkumar, G.P. Kalaignan and T. Vasudevan, *J. Power Sources* **75** (1998) 90.
16. S.U. Falk and A.J. Salkind, 'Alkaline Storage Batteries' (J. Wiley & Sons, New York, 1969), p. 240.
17. J. McBreen and E. Gagnon, *Electrochim. Acta* **26** (1981) 1439.
18. R. Othman, A.H. Yahaya and A.K. Arof, *J. New Mat. Electrochem. Systems*, **5** (2002) 177.
19. A. Duffield, P.J. Mitchell, D.W. Shield and N. Kumar, *in* L.J. Pearce (Ed.), 'Power Sources 11', International Power Sources Symposium Committee (Leatherhead, UK, 1987), p. 253.
20. Lucas Industries Ltd, *US Patent 4 407 915* (1983).
21. K. Bass, P.J. Mitchell, G.D. Wilcox and J. Smith, *J. Power Sources* **24** (1988) 21.
22. R. Othman, A.H. Yahaya and A.K. Arof, *in* O. Savadogo (Ed.), 'New Materials for Electrochemical Systems IV', Extended Abstract of the 4th International symposium on 'New Materials for Electrochemical Systems', 9–13 July 2001, Montreal, Quebec, Canada (Ecole Polytechnique de Montreal, 2001) p. 300.
23. R. Falshaw, R.H. Furneaux and D.E. Stevenson, *Carbohydr. Res.* **308** (1998) 107–115.
24. E. Marinho-Soriano, *J. Biotechnol.* **89** (2001) 81–84.
25. P. Singleton and D. Sainsbury, 'Dictionary of Microbiology and Molecular Biology', 2nd edn (J. Wiley & Sons, 1988), p. 19.
26. H.W. Ockerman, 'Source Book for Food Scientists' (AVI Publishing Co. 1978), pp. 563–568.
27. T. Singh, 'Agar and Agar Production', Infofish Technical Handbook 7 (Infofish, 1992).
28. R. Chandra and R. Rustgi, *Prog. Polym. Sci.* **23** (1998) 1273.
29. D.W. McComsey, *in* D. Linden (Ed.), 'Handbook of Batteries', 3rd edn (McGraw-Hill, New York, 2002), 8.1.
30. R.F. Scarr, J.C. Hunter and P.J. Slezak, *in* D. Linden (Ed.), *op. cit.* [29], 10.1.
31. N.C. Cahoon and H.W. Holland, *in* G.W. Heise and N.C. Cahoon (Eds), 'The Primary Battery', Vol. 1 (J. Wiley & Son, New York, 1971), p. 239.
32. C.K. Morehouse, R. Glicksman and G.S. Lozier, *in* S.N. Levine (Ed.), 'New Techniques for Energy Conversion' (Dover Publications, New York, 1961), p. 358.
33. R.P. Hamlen and T.B. Atwater, *in* D. Linden (Ed.), *op. cit.* [29], 38.1.
34. T.R. Crompton, 'Battery Reference Book', 3rd edn (Newnes, 2000), p. 26/3.
35. A.J. Appleby and M. Jacquier, *J. Power Sources* **1** (1976/77) 17.
36. D.A.J. Rand, *J. Power Sources* **4** (1979) 101.
37. J. McBreen *in* J.O'M. Bockris, B.E. Conway, E. Yeager and R.E. White (Eds), 'Comprehensive Treatise of Electrochemistry', Vol. 3 (Plenum Press, New York, 1981), p. 303.
38. R. Othman, W.J. Basirun, A.H. Yahaya and A.K. Arof, *J. Power Sources* **103** (2001) 34.
39. V.S. Bagotzky and A.M. Skundin, 'Chemical Power Sources' (Academic Press, New York, 1980), p. 242.
40. M.P. Vinod and K. Vijayamohanan, *J. Power Sources* **89** (2000) 88.
41. I. Lakatos and J. Lakatos-Szabo, *Colloids Surf. A* **141** (1998) 425.
42. D.M. Concidine (Ed.), 'Van Nostrand's Scientific Encyclopedia', 6th edn (Van Nostrand Reinhold, Princeton, NJ, 1983), pp. 907–909 and 1437.
43. McGraw-Hill 'Encyclopedia of Science and Technology', D.N. Lapedes (Editor-in-Chief), Vol. 1 (McGraw-Hill, New York, 1977), p. 128.
44. J.V. Smith (Ed.), 'X-Ray Powder Data File', Inorganic volume (ASTM, 1967), 5-0664.
45. M. Izaki and T. Omi, *J. Electrochem. Soc.* **144** (1997) 1949.
46. J.R. Goldstein, I. Brown and B. Koretz, *J. Power Sources* **80** (1999) 171.